NANO LETTERS

Letter

pubs.acs.org/NanoLett

Tailoring the Physical Properties of Molybdenum Disulfide Monolayers by Control of Interfacial Chemistry

Sina Najmaei,[†] Xiaolong Zou,[†] Dequan Er,[‡] Junwen Li,[‡] Zehua Jin,[§] Weilu Gao,[§] Qi Zhang,[∥] Sooyoun Park,[†] Liehui Ge,[†] Sidong Lei,[†] Junichiro Kono,[§,∥] Vivek B. Shenoy,[‡] Boris I. Yakobson,[†] Antony George,*[,†] Pulickel M. Ajayan,*[,†] and Jun Lou*[,†]

[†]Department Materials Science and NanoEngineering, Rice University, Houston, Texas 77005, United States

[‡]Materials Science and Engineering, University of Pennsylvania, 3231 Walnut Street, Philadelphia, Pennsylvania 19104, United States

[§]Department of Electrical and Computer Engineering and [∥]Department of Physics and Astronomy, Rice University, Houston, Texas 77005, United States

S *Supporting Information*

ABSTRACT: We demonstrate how substrate interfacial chemistry can be utilized to tailor the physical properties of single-crystalline molybdenum disulfide (MoS_2) atomic-layers. Semiconducting, two-dimensional MoS_2 possesses unique properties that are promising for future optical and electrical applications for which the ability to tune its physical properties is essential. We use self-assembled monolayers with a variety of end termination chemistries to functionalize substrates and systematically study their influence on the physical properties of MoS_2. Using electrical transport measurements, temperature-dependent photoluminescence spectroscopy, and empirical and first-principles calculations, we explore the possible mechanisms involved. Our data shows that combined interface-related effects of charge transfer, built-in molecular polarities, varied densities of defects, and remote interfacial phonons strongly modify the electrical and optical properties of MoS_2. These findings can be used to effectively enhance or modulate the conductivity, field-effect mobility, and photoluminescence in MoS_2 monolayers, illustrating an approach for local and universal property modulations in two-dimensional atomic-layers.

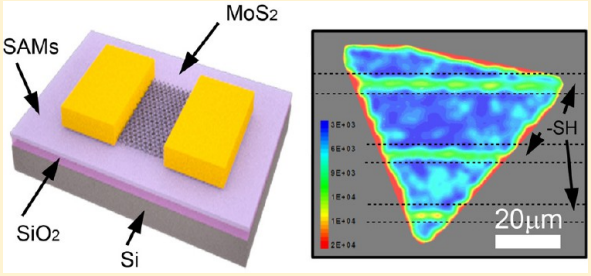

KEYWORDS: *Molybdenum disulfide, self-assembled monolayers, interface engineering, electronic transport, photoluminescence*

Recently, atomically thin two-dimensional monolayers of MoS_2 have attracted considerable research interest due to their appealing electrical and optical properties.[1−6] Reasonable carrier mobility, 1−40 ($cm^2/(V\ s)$), superior immunity to short channel effects,[2,7] and excellent photoresponse[3] renders MoS_2 as an ideal candidate for ultrathin electronics and photodetectors. Because of the presence of a direct bandgap in the electronic structure of MoS_2 and a consequentially higher on−off current ratio, it is a more suitable material for field effect devices as compared to graphene. Additionally, the existence of exotic physics of highly correlated systems such as valley-electronics,[4−6,8] defect-induced magnetism,[8] and metal insulator transitions[9,10] in MoS_2 promise possibilities beyond the aforementioned traditional semiconducting applications. Consequently, considerable research efforts have recently been made in large area synthesis and device prototyping.[11−16] In order to realize MoS_2-based devices, it is equally important to design strategies to control and tune its electrical and optical properties. In this effort, most of the attention has been focused on understanding top-gating mechanisms using high dielectric materials in order to screen substrate charge effects and enhance the gating process.[2,10] However, little has been done to understand, control, and modulate the electrical and optical properties of MoS_2 atomic layers by manipulating its substrate interactions.

Interface engineering has long been explored in two-dimensional electron gas systems and organic semiconductors as avenues for the development of new physics.[17−19] Previous studies on graphene suggest that the electrical properties of this 2D material can be tailored using its interaction with different substrate species.[20−23] Properties of MoS_2 are also not independent of substrate effects, and recent reports have indeed shown that the electrical properties of MoS_2 can be greatly influenced by the characteristics of its underlying substrate.[24−26] A theoretical study by Dolui et al. suggests that, depending on the surface conditions, MoS_2 on an SiO_2 substrate can show either p- or n-type carrier behavior.[25] It is believed that charge traps on the SiO_2 surfaces and random natural defects, namely siloxane (Si−O−Si) and silanol (Si−OH) groups, as well as impurity atoms such as sodium or potassium, mainly contribute to the variations in the electrical

Received: November 26, 2013
Revised: January 28, 2014
Published: February 11, 2014

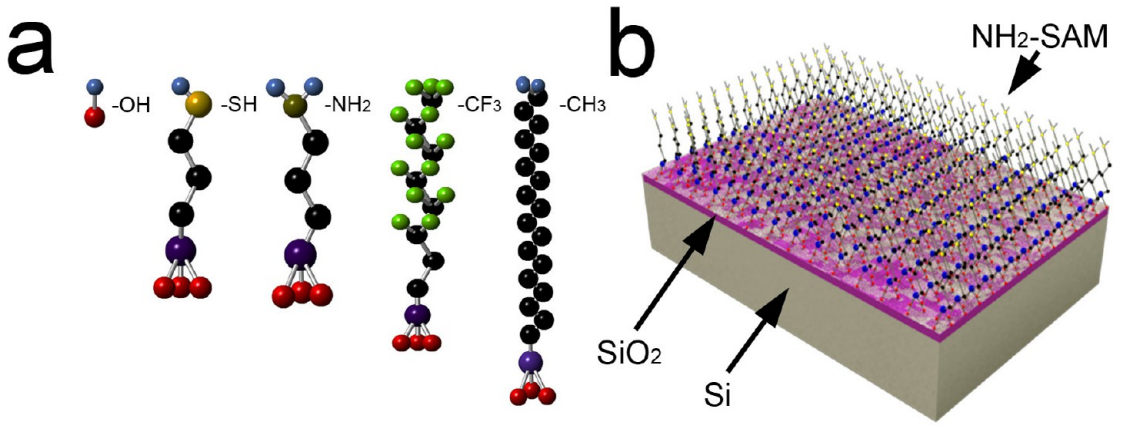

Figure 1. SAMs and substrate surface chemistry modulations. (a) The ball-and stick-models for SAMs used in the surface functionalization and their orientation relative to MoS_2 monolayers. (b) The assembled configuration of NH_2-SAM molecules as an example of surface functionalization.

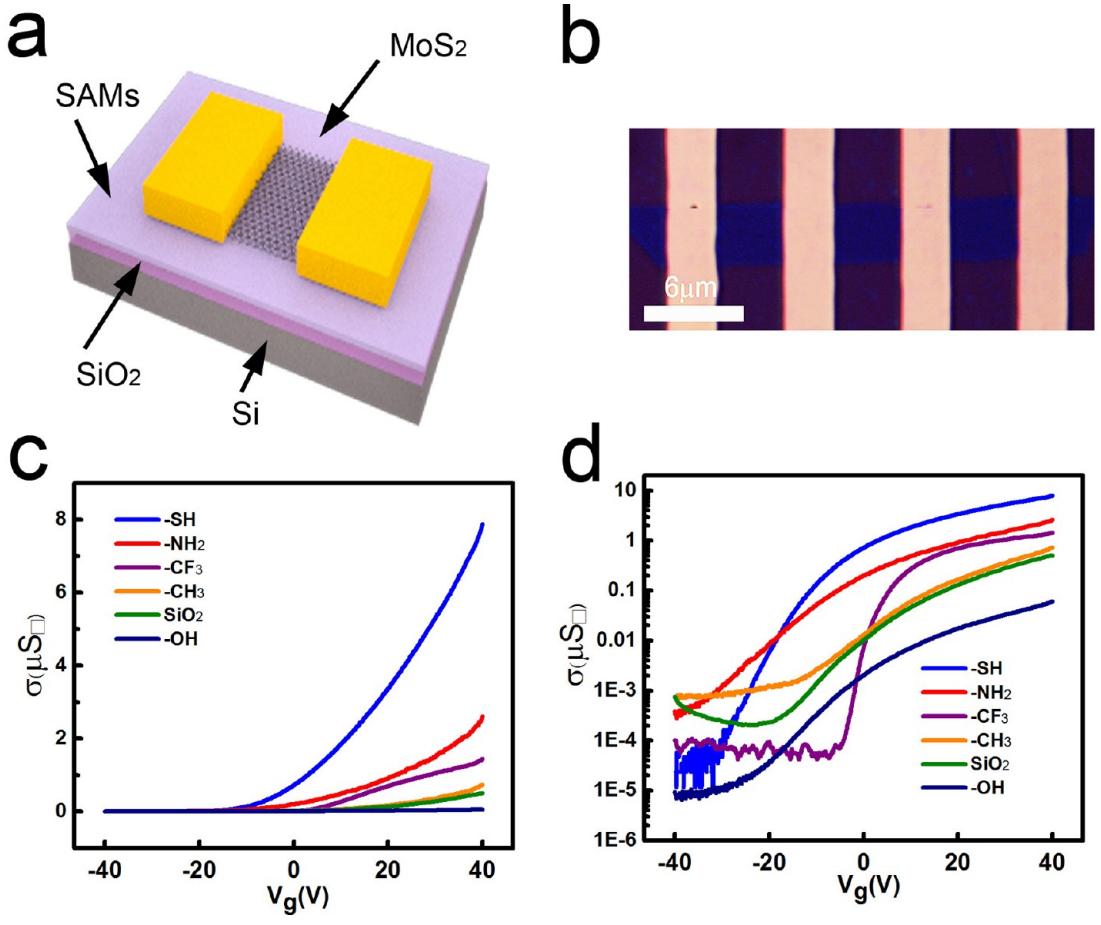

Figure 2. MoS_2 devices and transfer curves for varied substrates. (a,b) The schematic and top view optical micrograph of the device configurations in our experiments. (c) Transfer curves of representative measurements on a variety of modified and pristine substrates showing the ON-current modulation through interface engineering. Several important transport characteristics such as mobility, charge carrier mobility, threshold voltage, conductivity, and subthreshold swing can be estimated from these measurements. (d) Logarithmic scale presentation of the same measurements demonstrating the subthreshold device behavior as a function of substrate chemistry.

properties.[25] However, experimental realizations of such effects giving insight into the interface properties still remain.

Here, we report a surface-chemistry-based approach to effectively control the electrical and optical properties of MoS_2. We explore the SiO_2 gate oxide surfaces, functionalized with various self-assembled monolayers (SAMs), as platforms for controlled tuning of electronic and optical properties of MoS_2. We demonstrate that surface functionalization approaches can be utilized to tailor physical properties of MoS_2 including field-effect mobility, current density, threshold voltage, photoluminescence (PL) intensity, PL peak position, and PL line-width. Through empirical and analytical models combined with temperature-dependent measurements, we further reveal that these effects are primarily caused by charge

dx.doi.org/10.1021/nl404396p | Nano Lett. 2014, 14, 1354−1361

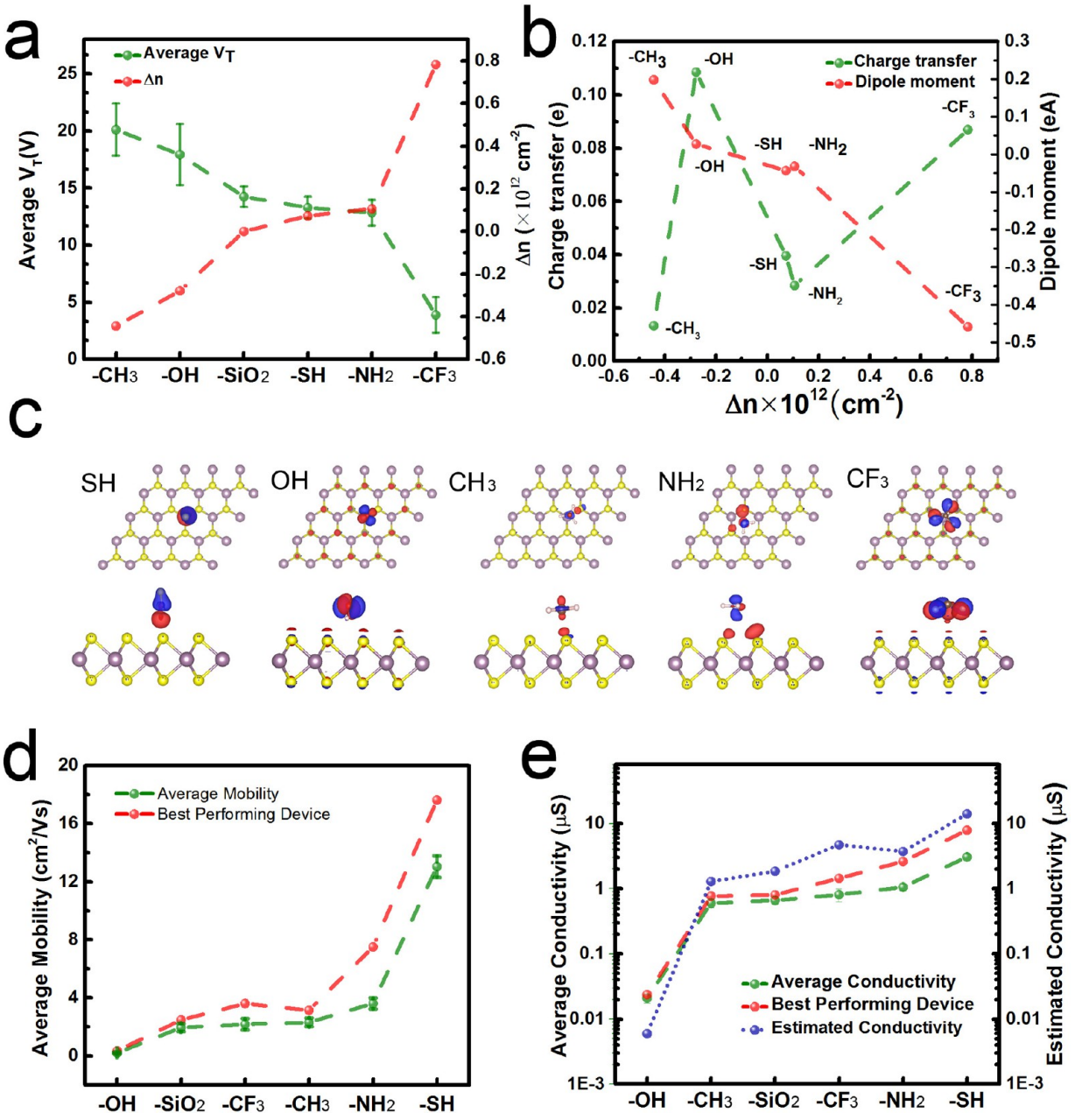

Figure 3. Device properties of samples on different substrates. (a) The changes in threshold voltage of MoS_2 devices made on varied substrates and the estimated charge carrier density changes as compare to samples on pristine SiO_2. (b) Estimated charge transfer between the substrate, MoS_2, and interface and the dipole moment in different SAM substrates. (c) Charge transfer and redistribution at the MoS_2 SAMs interface. The charge is transferred from the blue regions to the red. (d) Changes in the field effect mobility of MoS_2 samples on varied substrates and the best performing devices. (e) Changes in the conductivity of devices made of varied substrates represented by the average conductivity of all devices and best performing device gated at +40 V. The estimated conductivity is calculated form the Drude model for conductivity.

transfer, built-in molecular polarities, changes in substrate defect densities, and phononic interactions.

To examine the role of substrate chemistry on the electrical and optical properties of MoS_2, we prepared a variety of SAM-coated substrates with different surface chemistries, as described in the Supporting Information. These include: amine ($-NH_2$), methyl ($-CH_3$), fluoro ($-CF_3$), and thiol ($-SH$) functional groups (Figure 1a). Additionally, as control groups, we prepared pristine SiO_2 with natural defects and hydroxylated ($-OH$ functionalized) SiO_2 substrates. After the self-assembly of these organic monolayers (Figure 1b), high-quality, single-crystalline MoS_2 monolayers, synthesized using a previously reported recipe were transferred to these substrates.[15] After basic characterization using optical microscopy and Raman spectroscopy (Supporting Information Figure S1), MoS_2 field-effect devices, suitable for transport studies with a general configuration presented in Figure 2a,b, were prepared.

As the surface chemistry of the samples is modified, we anticipate four major changes and interactions that should affect our measurements: (i) charge transfer, (ii) built-in molecular polarities, (iii) modified substrate defect properties, and (iv) interfacial phononic property variations. We will initially focus on discussing substrate-dependent properties of

dx.doi.org/10.1021/nl404396p | Nano Lett. 2014, 14, 1354−1361

MoS_2 and then examine possible explanations for these observations.

The transfer curves acquired from our transport measurements demonstrate considerable tunability in MoS_2 conductivity and field-effect characteristics as substrate chemistry is modified (Figure 2c). The results show a highly controlled and smooth relationship between the MoS_2 field-effect characteristics and the substrate chemistry. Devices made on substrates with −OH termination showed the poorest conductivity and field-effect properties, while devices on −SH-terminated substrates showed the best performance with a 130-fold higher conductivity. As compared to devices on pristine SiO_2, a conductivity increase by about 15-fold was measured for devices on −SH treated substrates. The logarithmic scale transfer curves shown in Figure 2d reveal distinctive subthreshold behaviors. Devices on −OH, −SH, and $-CF_3$ terminated substrates showed low leakage currents, whereas devices on $-NH_2$ and $-CH_3$ substrates and pristine SiO_2 showed higher OFF current leakage, roughly 1 order of magnitude larger. These results demonstrate that devices on −SH and $-CF_3$ terminated substrates show the best subthreshold field-effect characteristics with a lower subthreshold swing and low OFF current (further discussions on the subthreshold behavior of MoS_2 is provided in Supporting Information).

To elucidate the role of surface chemistry in the transport properties of MoS_2, we estimate several important field-effect characteristics of the devices from gate-dependent conductance measurements presented in Figure 2c,d. The threshold voltage (V_T) shows positive values for all the samples (Figure 3a), ranging from ∼20 to 3 V. From the V_T variations, one can roughly estimate the changes in charge carrier densities as compared to pristine substrates, using the parallel plate capacitor model. In this model, one can use the relationship $n = C_{ox}\Delta V_T/e$ to estimate the charge concentration changes as compared to SiO_2. Here, C_{ox} is the capacitance of the SiO_2, $\Delta V_T = V_{T,SAM} - V_{T,SiO2}$, and $e = 1.602 \times 10^{-19}$ C is the elementary charge. In this estimation, the thickness of the SAMs range between 0.5 and 1.2 nm[27,28] and have dielectric constants in the range of 2−3.[27,28] Therefore, the capacitance contribution of the SAMs can be ignored and the charge carrier density can be calculated based only on the SiO_2 parameters. The capacitance is estimated from $C_{ox} = \varepsilon_0\varepsilon_r/d_{ox}$, where $\varepsilon_0 = 8.85 \times 10^{-12}$ Fm^{-1}, ε_r for SiO_2 is 3.9, and d_{ox} = 285 nm. The estimated changes in charge carrier density for samples on different SAM substrates are shown in Figure 3a. This level of V_T tunability in MoS_2 implies remarkable interface physics linked to the diverse surface chemistries. For in-plane transport in 2D devices based on MoS_2, two transport channels for charge carriers can exist: the MoS_2 conduction band, which mainly lies in the MoS_2 2D plane, and the interface states that are distributed between MoS_2 and the substrates. Having this configuration in mind, we first calculate the charge transfer properties of MoS_2 and its substrates based on density functional theory (DFT). In almost all cases, the interactions between the material and its substrates result in charge transfer from both the SAMs and MoS_2 to the interface and charge redistribution, giving rise to a significant increase in the interface charge carrier density (Figure 3b,c). The net charge transfers are shown in Figure 3b and the charge distributions depicted in Figure 3c. Governed by the nature of interface states and their enhanced scattering mechanisms, the carriers at the interface are less mobile and contribute little to the transport, when compared to MoS_2 channel. If charge transfer was the only contributor, the overall transport properties of all devices would have degraded. However, by calculating the dipole moment along the molecular chains for different substrates, as shown in Figure 3b, an important distinction among substrates with different built-in dipoles is apparent. The molecular dipole fields influence the tunneling of charge carriers between the trap interface states and MoS_2 conduction channel. In cases where the dipole moment is positive, the interface charge carrier density is further enhanced as the molecular field accumulates more charge in the interface and further depletes the MoS_2 conduction channel. This is why those substrates with the most positive dipoles ($-CH_3$ and −OH) show the lowest carrier densities, while in those with negative dipoles ($-NH_2$, −SH, and $-CF_3$), the charge carriers in the interface are pushed into the MoS_2 channel and the charge carrier density increases as the bias voltage is applied. It is evident that this behavior closely follows the magnitude and direction of dipole moments, and bias-dependent experiments further confirm our model (Figure 3a,b and Supporting Information Figure S2d). Additionally the hysteresis, calculated from the forward and reverse transfer curves in Supporting Information Figure S3 for devices made on $-CH_3$, $-SiO_2$, and −OH with values 7.8, 7.6, and 13.4 V, respectively, is significantly higher than devices made on −SH, $-NH_2$, and $-CF_3$ with values 4.5, 3.01, and 3.6 V, respectivly. This confirms that the density of trap sites in these substrates is higher and confirms our previous observations.

Estimating the charge carrier mobilities in the devices can further elucidate the physics involved. From the transfer curves measured for each device, one can estimate the charge carrier mobility from the linear region of the transfer curves using the equation described in the Methods section. The average MoS_2 field effect mobility on functionalized substrates is presented in Figure 3d. These results show a continuous increase in mobility from −OH to −SH substrates. A significant enhancement, by roughly 6.7-fold, in the mobility of devices made on −SH (13.0 $cm^2/(V\ s)$) as compared to the pristine substrate (1.9 $cm^2/(V\ s)$) is observed. Charge carrier mobility in its fundamental level can be influenced by changes in the scattering properties of the system, by changes in the effective mass of the charge carriers, or by both. Other than the small material strain due to the lattice mismatch between MoS_2 and its substrate, major alterations in the band structure of the material is not expected on different substrates. Therefore, changes in the material mobility on different substrates can be attributed to the modified density of defects, trap states, and interfacial phononic interactions.

It is instructive to estimate the conductivity of the devices on different substrates and extract the carrier density and mobility trends. We measure the average conductivity of devices made on different substrates at V_g = 40 V presented in Figure 3e. One can observe a significant device conductivity dependence on the substrate properties. A major enhancement, roughly 3 orders of magnitude, in the conductivity from devices made on −OH to those on −SH substrates is observed. The best-performing device on SH-SAMs shows a conductivity of roughly 8 μS, which is approximately 4.6-fold larger than samples on SiO_2. The conductivity in the diffusive regime has a linear relationship with charge carrier density and mobility which can be expressed by $\sigma = ne\mu$, where n is the charge carrier density, e is the electronic charge, and μ is the charge carrier mobility. We can estimate n from the values in Figure 3a,

dx.doi.org/10.1021/nl404396p | Nano Lett. 2014, 14, 1354−1361

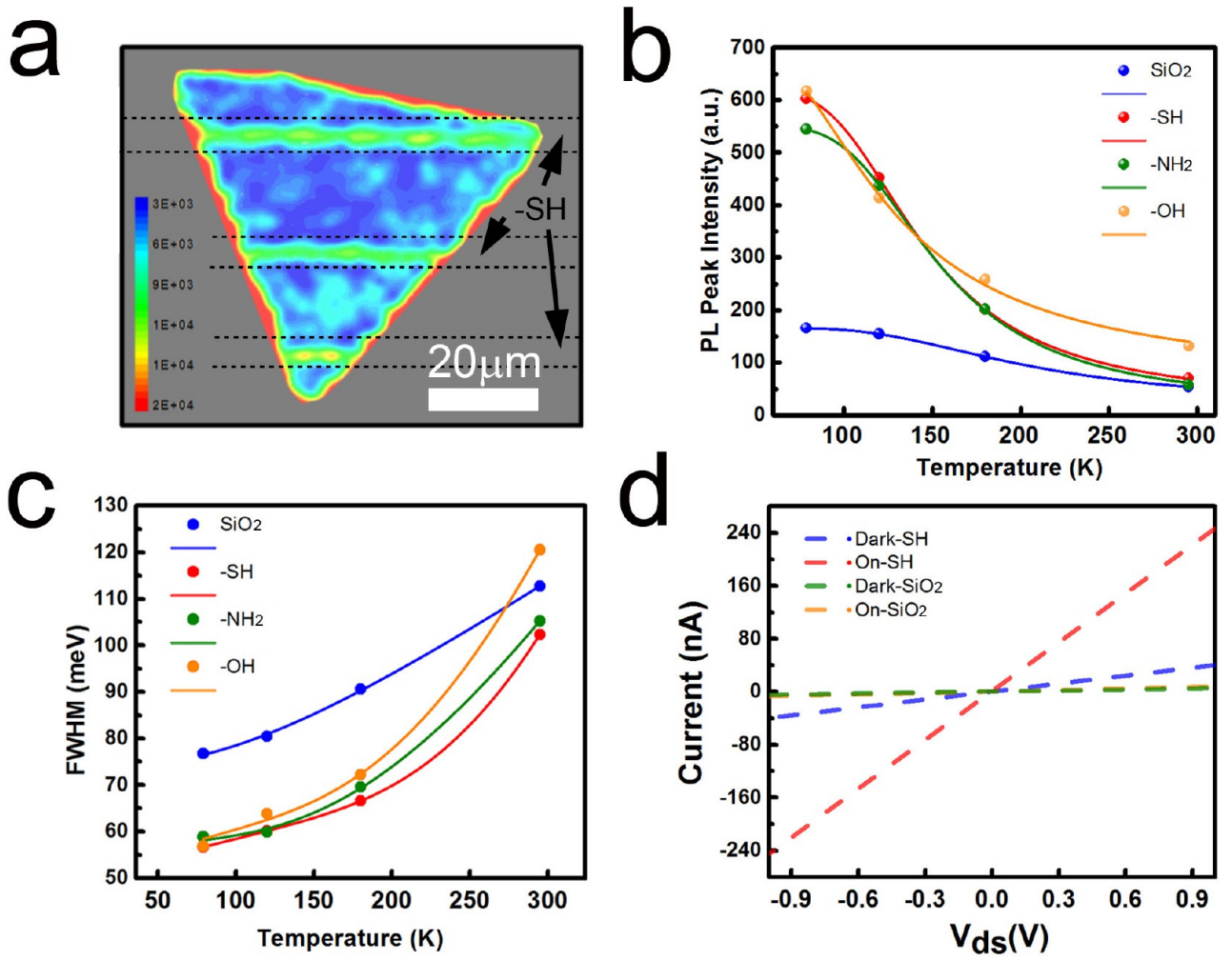

Figure 4. Photoluminescence and photoconductivity on varied substrates. (a) PL intensity map at 673 nm on patterned SH-SAMs using 2.5 mW power. The dashed lines distinguish the underlying −SH patterns. The region outside the triangle does not fluorescence which eliminates the possibility that the PL is from the substrate or SH-SAMs. Temperature dependence of (b) the PL intensity, (c) the PL line-width (full width at half-maximum) for MoS_2 on different substrates. (d) Current−voltage curves for MoS_2 on SiO_2 and SH-SAMs under dark conditions and under photoexcitation using 532 nm wavelength at laser power of 60 μW.

assuming that $n_o = 5 \times 10^{12}$ cm^{-2} (similar to MoS_2 residual carrier density reported in the literature[10]). The results acquired from this classical model perfectly match the experimental results, confirming our estimations for the charge carrier density and mobility changes. Therefore, we can conclude that in order to explain the performance of the devices on different SAMs, a combination of charge carrier density and mobility changes play a considerable role. For instance, the maximum enhancement in device conductivity observed in devices made on −SH and $-NH_2$ functionalized substrates is primarily attributed to the changes in charge carrier mobility, as the changes in charge carrier density for these samples are negligible (Figure 3e). However, for −OH substrates with low charge carrier mobilities and densities, a collectively low conductivity is expected.

Next, we examine the influence of interactions with the substrate on the optical properties of MoS_2 using PL mapping and temperature-dependent PL measurements on a subset of our samples. We measure the PL from single flakes of MoS_2 monolayers on four different substrates at different temperatures (see Supporting Information for the actual spectra). The most intense PL peak, observed at ∼1.92 eV, is due to the A exciton, while a weaker PL peak, due to the B exciton, is observed at ∼2.08 eV. These transitions are associated with the direct optical transitions between the bottom of the conduction band and the top of the (spin−orbit−split) valence band.[1] We used patterned SAMs to locally modifying surface chemistry and inspect the photoluminescence intensity changes in large MoS_2 single crystalline nanosheets. For this, SAM photolithography pattering approaches were used to prepare thiol (−SH) terminated line arrays (6 μm wide and 15 μm apart) (Figure 4a). The PL intensity maps at 673 nm, acquired from MoS_2 nanosheets transferred to the patterned substrates, show a considerable local intensity modulation, by roughly 4.4-fold at the -SH modified as compared to pristine SiO_2 areas. Therefore, Figure 4a demonstrates an easy approach for local modulation MoS_2 optical properties using SH-SAMs. The area selective modulation of physical properties of layered materials demonstrated here are technologically and scientifically important, since such approaches may lead to remarkable physical phenomenon and device possibilities. It has been demonstrated that doping and dielectric environment can affect the PL intensity and peak positions of MoS_2;[29,30] specifically, the PL intensity increases as the Fermi level is lowered or the

dx.doi.org/10.1021/nl404396p | Nano Lett. 2014, 14, 1354−1361

dielectric constant of the substrate decreases.[29,30] However, our observations, described in detail below, cannot be explained using only these general characteristics, requiring explanations beyond these effects.

To decipher the underlying physics involved in PL intensity modulations, we perform temperature-dependent PL studies. The temperature-dependent measurements in Figure 4b show that the PL intensity has strong substrate dependence, especially at low temperatures. At room temperature, all the samples on surface functionalized substrates show higher PL intensities, as compared to that on pristine SiO_2. These differences are less discernible than the PL map measurements, due to the lower intensity of the laser, by roughly 1 order of magnitude. However, it is sufficient for understanding the underlying physics as temperature is decreased. At 79 K, the PL of all samples on functionalized substrates have similar intensities, approximately 3.5 times larger than that of MoS_2 on pristine SiO_2. The decrease in PL intensity with increasing temperature is believed to be due to thermal activation of nonradiative recombination centers.[31] In fact, the observed temperature dependence of the PL intensity (Figure 4b) can be well fitted with the equation $I(T) = I_0/[1 + A \exp(-E_a/k_BT)]$. The values for the thermal activation energy, E_a, extracted through fitting, ranged from 30 to 60 meV in our samples. Additionally, the higher values of I_0 obtained for the samples with functionalized substrates imply that these treated substrates have fewer defects with more uniform lattice potentials as compared to pristine SiO_2, because the internal defect densities in CVD-grown samples, mainly sulfur vacancies, are known to be rather uniform.[32]

The temperature dependence of the PL peak position (Supporting Information Figure S6b) can be fitted with a modified Varshni relationship, $E_g(T) = E_g(0) - S\langle\hbar\omega\rangle[\coth(\langle\hbar\omega\rangle/2k_BT) - 1]$,[33,34] where S is a coupling constant describing electron−phonon interactions, $\langle\hbar\omega\rangle$ is the average energy of acoustic phonons, and the $\coth(\langle\hbar\omega\rangle/2k_BT)$ expresses the density of phonons as a function of temperature. Fitting the experimental results in Supporting Information Figure S6b with this model does not show much difference between the different samples, suggesting that the intrinsic band structure itself is not affected by the different substrates.

Figure 4c shows the temperature dependence of the PL line-width, which can be fitted with the following equation: $\Gamma(T) = \Gamma_0 + \gamma_{ph}T + \Gamma_{LO}/[\exp(\hbar\omega_{LO}/k_BT) - 1]$, where $\hbar\omega_{LO}$ is the average longitudinal optical (LO) phonon energy, Γ_0 is the broadening parameter at 0 K, γ_{ph} is the exciton-acoustic phonon scattering rate, and Γ_{LO} is the exciton-optical phonon scattering rate. In addition, scattering by remote interfacial phonons (RIP), that is, polar optical phonons of the substrate, need to be taken into account.[22] The change in $T = 0$ line-width Γ_0 from modified substrate to SiO_2 can be attributed to extrinsic scattering related to the substrate and its defect, and the decrease in this value by about 20−30% from pristine to functionalized substrates suggests significantly modified interactions between excitons and the substrate. From the linear-T dependence in the low-temperature region, we can estimate γ_{ph} to be 0.189, 0.196, 0.134, and 0.277 μeV/K, respectively, for the samples on SiO_2, $-NH_2$, $-SH$, and $-OH$; these values are comparable, and thus, the major difference in PL line-width must come from interactions with LO and RIP modes at temperatures higher than 100 K.[22] The generally lower line width for the modified substrates can be explained by the expected higher optical phonon energies in SAMs bearing in mind their stronger bonding properties as compared to SiO_2. These findings can be extrapolated to our electrical observations and one can conclude that the role of substrate optical phonon and defect properties is seminal in tailoring the optical and electrical properties of MoS_2. As shown in Figure 4d, the photoresponse of devices made on $-SH$ substrates can be enhanced by 4-fold compared to samples on SiO_2. This can be attributed to the complementary enhancements in optical and electrical properties of devices made on $-SH$ substrates.

In summary, we demonstrate a feasible approach for the systematic modification of MoS_2 electrical and optical properties through interface engineering. This approach illustrates a systematic area selective route that allows for electronic and photonic control of MoS_2 properties. We provide a comprehensive understanding of the substrate role in properties of MoS_2 by examining the possible interactions and underlying physics involved. We explain that a combined effect of charge transfer, molecular polarities of surface functional groups, variations in surface defect properties, and phononic interactions control MoS_2 electrical and optical properties. Our results illustrate how precise interface engineering can be used as an effective way for physical property modulation in 2D materials.

Methods. *Device Fabrication.* The MoS_2 nanosheets were transferred to the variety of substrates by a common polymer base transfer approach. Using conventional photolithography processes followed by e-beam evaporation, the field effect devices were prepare on the single crystalline triangular MoS_2 domains. For the lithography process we used photoresist S1813 and LOR5B as an adhesive layer, and mask aligner (SUSS Mask Aligner MJB4). Ti/Au (4 nm/36 nm) were used for metallization of photolithography patterns and to fabricate the source and drain electrodes. Finally, using a second photolithography and plasma etching step, the MoS_2 triangles were cut into uniform rectangular sheets with a length to width ratio of ∼1 using O_2 reactive ion etching (RIE, Phantom III). The photoresist is removed by acetone and PG-REMOVER. Using this technique over 90 devices were fabricated and tested.

Transport Measurements. All electrical measurements are performed in a Lakeshore probe station under vacuum conditions ($<10^{-5}$ Torr) to minimize environmental effects. These devices were analyzed using an Agilent B1500A Semiconductor Device Analyzer. All together more than 250 devices were investigated. We performed transport measurements under vacuum conditions (10^{-5} Torr) on different types of chemically modified and pristine substrates. The measurements were performed with an applied gate voltage ranging from −40 to 40 V.

MoS_2 Field Effect Mobility Estimation. To estimated the field effect mobility of devices we use $\mu = [dI_{ds}/dV_{bg}] \times [(L/WC_iV_{ds})]$, where L and W are the channel length and width. The capacitance between the channel and the back gate per unit area is estimated to be $\sim 1.2 \times 10^{-4}$ Fm^{2-} ($C_i = \varepsilon_0\varepsilon_r/d$, where $\varepsilon_0 = 3.9$ and $d = 285$ nm).

Molecular Dipole and Charge Transfer Calculations. The molecular dipoles are calculated employing the Perdew−Burke−Ernzerhof (PBE)[35] parametrization of the generalized gradient approximation potential. For the charge transfer calculations, we performed spin-polarized density functional calculations with PBE[35] approximation for exchange correlation functional. The Mo[4p5s4d], S[s2p4], N[s2p3], C[s2p2], and F[s2p5] were explicitly considered as valence electrons whose

dx.doi.org/10.1021/nl404396p | Nano Lett. 2014, 14, 1354−1361

interaction with ion cores was modeled by projector augment wave method.[36,37]

PL Measurements. PL measurements were performed by focusing the laser radiation centered at 514 nm from an argon-ion laser onto the single MoS_2 monolayer flake via a 50× objective lens. The laser excitation power was about 200 μW at the sample. The reflectance radiation was collected and analyzed with a grating spectrometer equipped with a liquid nitrogen cooled charge-coupled device camera. Low-temperature PL measurements were performed by using a continuous flow liquid nitrogen cryostat. The PL maps were acquired using a Renishaw PL/Raman microscope using a 514 nm laser at 2.5 mW.

■ ASSOCIATED CONTENT

Supporting Information

Description of SAM preparation and characterization, Raman and PL characterization of as grown MoS_2, discussions on subthreshold characteristics, charge transfer, dipole properties, and analysis of device hysteresis, as well as supplementary figures. This material is available free of charge via the Internet at http://pubs.acs.org.

■ AUTHOR INFORMATION

Corresponding Authors

*(A.G.) E-mail: antony.utwente@gmail.com.
*(P.M.A.) E-mail: ajayan@rice.edu.
*(J.L.) E-mail: jlou@rice.edu.

Author Contributions

S.N., A.G., P.M.A., and J.L. conceived the idea and designed the experiments. S.N. and S.P. synthesized the MoS_2 samples. S.N. and A.G. prepared the SAMs substrates and devices and performed the electrical transport measurements. D.E. and J.L. performed the charge transfer calculations. X.Z. performed the dipole calculation and helped with the data analysis. S.N. obtained the PL map. S.N., S.L., and L.G. performed the photocurrent measurements. Z.J., W.G., and Q.Z. performed the PL measurements. S.N. and A.G. analyzed all data. J.K., V.B.S., A.G., P.M.A., and J.L. supervised the work. S.N., A.G., P.M.A., and J.L. wrote the paper and all authors discussed and revised the final manuscript.

Notes

The authors declare no competing financial interest.

■ ACKNOWLEDGMENTS

This work was supported by the Robert A. Welch Foundation Grants C-1716 and C-1509, the NSF Grants ECCS-1327093, ECCS-0928297, the U.S. Army Research Office MURI Grants W911NF-11-1-0362, the U.S. Office of Naval Research MURI Grant N000014-09-1-1066, and the Nanoelectronics Research Corporation contract S201006. A.G. acknowledges financial support from Netherlands organization for scientific research (NWO) under the framework of Rubicon program (project number 680-50-1205). V.B.S. gratefully acknowledges the support of the Army Research Office through contract W911NF-11-1-0171. S.E. and J.L. are supported by the NSF award CMMI 1308396.

■ REFERENCES

(1) Mak, K. F.; Lee, C.; Hone, J.; Shan, J.; Heinz, T. F. *Phys. Rev. Lett.* **2010**, *105* (13), 136805.
(2) Radisavljevic, B.; Radenovic, A.; Brivio, J.; Giacometti, V.; Kis, A. *Nat. Nanotechnol.* **2011**, *6* (3), 147−150.
(3) Lopez-Sanchez, O.; Lembke, D.; Kayci, M.; Radenovic, A.; Kis, A. *Nat. Nanotechnol.* **2013**, *8* (7), 497−501.
(4) Cao, T.; Wang, G.; Han, W.; Ye, H.; Zhu, C.; Shi, J.; Niu, Q.; Tan, P.; Wang, E.; Liu, B.; Feng, J. *Nat. Commun.* **2012**, *3*, 887.
(5) Mak, K. F.; He, K.; Shan, J.; Heinz, T. F. *Nat. Nanotechnol.* **2012**, *7* (8), 494−498.
(6) Zeng, H.; Dai, J.; Yao, W.; Xiao, D.; Cui, X. *Nat. Nanotechnol.* **2012**, *7* (8), 490−493.
(7) Liu, H.; Neal, A. T.; Ye, P. D. *ACS Nano* **2012**, *6* (10), 8563−8569.
(8) Mathew, S.; Gopinadhan, K.; Chan, T. K.; Yu, X. J.; Zhan, D.; Cao, L.; Rusydi, A.; Breese, M. B. H.; Dhar, S.; Shen, Z. X.; Venkatesan, T.; Thong, J. T. L. *Appl. Phys. Lett.* **2012**, *101* (10), 102103−5.
(9) Ye, J. T.; Zhang, Y. J.; Akashi, R.; Bahramy, M. S.; Arita, R.; Iwasa, Y. *Science* **2012**, *338* (6111), 1193−1196.
(10) Radisavljevic, B.; Kis, A. *Nat. Mater.* **2013**, *12* (9), 815−820.
(11) Zhan, Y.; Liu, Z.; Najmaei, S.; Ajayan, P. M.; Lou, J. *Small* **2012**, *8* (7), 966−971.
(12) Lee, Y.-H.; Zhang, X.-Q.; Zhang, W.; Chang, M.-T.; Lin, C.-T.; Chang, K.-D.; Yu, Y.-C.; Wang, J. T.-W.; Chang, C.-S.; Li, L.-J.; Lin, T.-W. *Adv. Mater.* **2012**, *24* (17), 2320−2325.
(13) Liu, K.-K.; Zhang, W.; Lee, Y.-H.; Lin, Y.-C.; Chang, M.-T.; Su, C.-Y.; Chang, C.-S.; Li, H.; Shi, Y.; Zhang, H.; Lai, C.-S.; Li, L.-J. *Nano Lett.* **2012**, *12* (3), 1538−1544.
(14) Li, X.; Cai, W.; An, J.; Kim, S.; Nah, J.; Yang, D.; Piner, R.; Velamakanni, A.; Jung, I.; Tutuc, E.; Banerjee, S. K.; Colombo, L.; Ruoff, R. S. *Science* **2009**, *324* (5932), 1312−1314.
(15) Najmaei, S.; Liu, Z.; Zhou, W.; Zou, X.; Shi, G.; Lei, S.; Yakobson, B. I.; Idrobo, J.-C.; Ajayan, P. M.; Lou, J. *Nat. Mater.* **2013**, *12* (8), 754−759.
(16) van der Zande, A. M.; Huang, P. Y.; Chenet, D. A.; Berkelbach, T. C.; You, Y.; Lee, G.-H.; Heinz, T. F.; Reichman, D. R.; Muller, D. A.; Hone, J. C. *Nat. Mater.* **2013**, *12* (6), 554−561.
(17) Nakagawa, N.; Hwang, H. Y.; Muller, D. A. *Nat. Mater.* **2006**, *5* (3), 204−209.
(18) Ohtomo, A.; Hwang, H. Y. *Nature* **2004**, *427* (6973), 423−426.
(19) Kobayashi, S.; Nishikawa, T.; Takenobu, T.; Mori, S.; Shimoda, T.; Mitani, T.; Shimotani, H.; Yoshimoto, N.; Ogawa, S.; Iwasa, Y. *Nat. Mater.* **2004**, *3* (5), 317−322.
(20) Lee, B.; Chen, Y.; Duerr, F.; Mastrogiovanni, D.; Garfunkel, E.; Andrei, E. Y.; Podzorov, V. *Nano Lett.* **2010**, *10* (7), 2427−2432.
(21) Yan, Z.; Sun, Z.; Lu, W.; Yao, J.; Zhu, Y.; Tour, J. M. *ACS Nano* **2011**, *5* (2), 1535−1540.
(22) Chen, J.-H.; Jang, C.; Xiao, S.; Ishigami, M.; Fuhrer, M. S. *Nat. Nanotechnol.* **2008**, *3* (4), 206−209.
(23) Meyer, J. C.; Geim, A. K.; Katsnelson, M. I.; Novoselov, K. S.; Booth, T. J.; Roth, S. *Nature* **2007**, *446* (7131), 60−63.
(24) Ayari, A.; Cobas, E.; Ogundadegbe, O.; Fuhrer, M. S. *J. Appl. Phys.* **2007**, *101* (1), 014507−5.
(25) Dolui, K.; Rungger, I.; Sanvito, S. *Phys. Rev. B* **2013**, *87* (16), 165402.
(26) Bao, W.; Cai, X.; Kim, D.; Sridhara, K.; Fuhrer, M. S. *Appl. Phys. Lett.* **2013**, *102* (4), 042104−4.
(27) Rampi, M. A.; Schueller, O. J. A.; Whitesides, G. M. *Appl. Phys. Lett.* **1998**, *72* (14), 1781−1783.
(28) Romaner, L.; Heimel, G.; Ambrosch-Draxl, C.; Zojer, E. *Adv. Funct. Mater.* **2008**, *18* (24), 3999−4006.
(29) Mak, K. F.; He, K.; Lee, C.; Lee, G. H.; Hone, J.; Heinz, T. F.; Shan, J. *Nat. Mater.* **2013**, *12* (3), 207−211.
(30) Komsa, H.-P.; Krasheninnikov, A. V. *Phys. Rev. B* **2012**, *86* (24), 241201.
(31) Zhang, X. T.; Liu, Y. C.; Zhi, Z. Z.; Zhang, J. Y.; Lu, Y. M.; Shen, D. Z.; Xu, W.; Fan, X. W.; Kong, X. G. *J. Lumin.* **2002**, *99* (2), 149−154.

(32) Zhou, W.; Zou, X.; Najmaei, S.; Liu, Z.; Shi, Y.; Kong, J.; Lou, J.; Ajayan, P. M.; Yakobson, B. I.; Idrobo, J.-C. *Nano Lett.* **2013**, *13* (6), 2615−2622.
(33) Varshni, Y. P. *Physica* **1967**, *34* (1), 149−154.
(34) O'Donnell, K. P.; Chen, X. *Appl. Phys. Lett.* **1991**, *58* (25), 2924−2926.
(35) Perdew, J. P.; Burke, K.; Ernzerhof, M. *Phys. Rev. Lett.* **1996**, *77* (18), 3865−3868.
(36) Kresse, G.; Joubert, D. *Phys. Rev. B* **1999**, *59* (3), 1758−1775.
(37) Blöchl, P. E. *Phys. Rev. B* **1994**, *50* (24), 17953−17979.